

# Solvent Effects on Degradative Condensation Side Reactions of Fructose in Its Initial Conversion to 5-Hydroxymethylfurfural

Xing Fu,<sup>[a]</sup> Yexin Hu,<sup>[a]</sup> Yanru Zhang,<sup>[a]</sup> Yucheng Zhang,<sup>[a]</sup> Dianyong Tang,<sup>[b]</sup> Liangfang Zhu,<sup>\*[a]</sup> and Changwei Hu<sup>\*[a]</sup>

The degradative condensation of hexose, which originates from the C–C cleavage of hexose and condensation of degraded hexose fragment, is one of the possible reaction pathways for the formation of humins in hexose dehydration to 5-hydroxymethylfurfural (HMF). Herein, the impacts of several polar aprotic solvents on the degradative condensation of fructose to small-molecule carboxylic acids and oligomers (possible precursors of humins) are reported. In particular, a close relationship between the tautomeric distribution of fructose in solvents and the mechanism of degradative condensation is dem-

onstrated. Typically,  $\alpha$ -fructofuranose in 1,4-dioxane and acyclic open-chain fructose in THF favor the conversion of fructose to formic acid and oligomers;  $\alpha$ -fructopyranose in  $\gamma$ -valerolactone or *N*-methylpyrrolidone favors levulinic acid and oligomers, whereas  $\beta$ -fructopyranose in 4-methyl-2-pentanone favors acetic acid and corresponding oligomers. This close correlation highlights a general understanding of the solvent-controlled formation of oligomers, which represents an important step toward the rational design of effective solvent systems for HMF production.

## Introduction

Lignocellulosic biomass is the most abundant and inexpensive renewable resource that can potentially substitute the fossil resources for producing transportation fuels and commodity chemicals.<sup>[1]</sup> Over the past decade, tremendous efforts have been made to develop effective methods to sustainably transform lignocellulosic biomass-derived feedstock into value-added products.<sup>[2a,b]</sup> Among others, 5-hydroxymethylfurfural (HMF), the dehydrated product of hexose, has been regarded as a key platform chemical.<sup>[3a–c]</sup> Nowadays, the highly selective synthesis of HMF by catalytic dehydration of hexose has attracted increasing attention.<sup>[4a,b]</sup> However, several side reactions are involved in hexose dehydration, which lowers the HMF selectivity and increases the separation energy. Large-scale industrialization of HMF is feasible but has not yet been realized;<sup>[5]</sup> this is mainly hampered by the formation of soluble or insoluble polymeric byproducts. Such undesirable carbonaceous substances account for 10–50% carbon loss of the feedstock, thereby decreasing the economic viability.<sup>[6a–c]</sup> To improve the

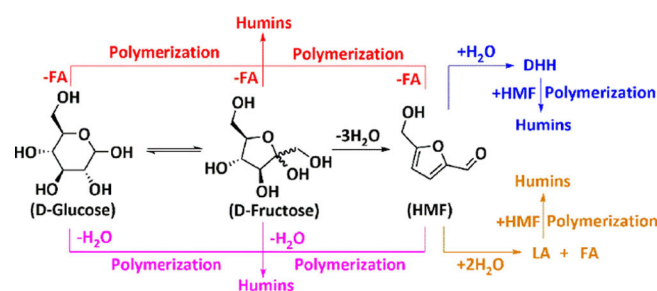
utilization of biomass-derived carbon resources, the formation of humins should be limited as much as possible.

An understanding of the reaction pathways of humin formation might be greatly helpful for its future inhibition. A schematic illustration of such formation pathways is exhibited in Scheme 1, wherein the condensation/polymerizations of partly dehydrated hexose and/or HMF are proposed to be responsible for humin formation.<sup>[7a–d]</sup> Significantly, HMF itself has been regarded as a key intermediate for humin formation through the uncontrolled self-<sup>[8]</sup> or cross-polymerization with other highly reactive intermediates [i.e., 2,5-dioxo-6-hydroxyhexanal (DHH)] and/or products [(i.e., levulinic acid (LA))] in aqueous solution.<sup>[9a–e]</sup> Based on this understanding, effective strategies have been developed to inhibit the rehydration of HMF to form DHH or LA through the rational design of catalysts<sup>[10a–e]</sup> and cautious selection of solvents,<sup>[11a–c]</sup> such that the formation of humins could be alleviated.

[a] Dr. X. Fu, Y. Hu, Y. Zhang, Y. Zhang, Dr. L. Zhu, Prof. C. Hu  
Key Laboratory of Green Chemistry and Technology  
Ministry of Education, College of Chemistry  
Sichuan University  
Chengdu, Sichuan 610064 (P.R. China)  
E-mail: zhulf@scu.edu.cn  
changwei.hu@scu.edu.cn

[b] Dr. D. Tang  
International Academy of Targeted Therapeutics and Innovation  
Chongqing University of Arts and Sciences  
Chongqing 402160 (P.R. China)

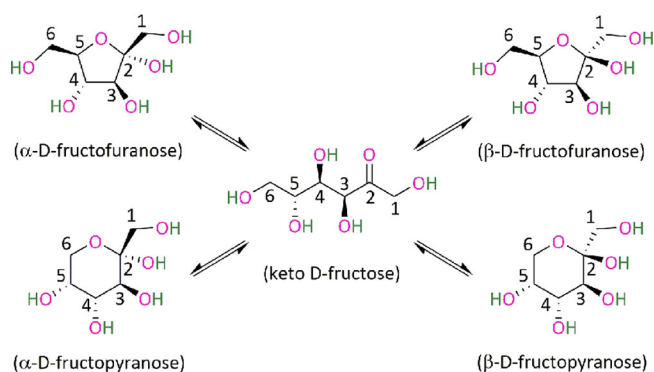
 Supporting Information and the ORCID identification number(s) for the author(s) of this article can be found under:  
<https://doi.org/10.1002/cssc.201902309>.



**Scheme 1.** Reaction pathways of humin formation during hexose dehydration. DHH = 2,5-dioxo-6-hydroxyhexanal, LA = levulinic acid, FA = formic acid.

However, humins might also be generated from the degradative condensation of glucose, fructose, and/or HMF. Herein, the concept of degradative condensation is proposed and defined as the oligomerization of the intermediates derived from the C–C cleavage of hexose or HMF. The degradative condensation of fructose might be easier than that of glucose and HMF, as proposed in our previous work.<sup>[12]</sup> Recent kinetic studies revealed that the apparent activation energy of the acid-catalyzed degradative condensation of fructose ranged from 79 to 130 kJ mol<sup>-1</sup>.<sup>[12,13a–c]</sup> Although a limited mechanistic understanding has been achieved, it is widely accepted that such degradative condensation produces oligomers associated with a degraded product, namely, formic acid (FA). The rehydration of HMF also generates equal molar amounts of FA and LA. Nevertheless, several studies have reported the formation of a stoichiometric excess of FA, relative to that of LA, during fructose dehydration in various solvents,<sup>[14a–f]</sup> which suggests the general existence of a degradative condensation route that might be related to humin formation. In this regard, developing mechanistic insights into how reaction parameters influence the degradative condensation of hexose is of critical importance for the design of optimal reaction systems to inhibit humin formation and then enhance HMF selectivity.

A wide range of solvents, including polar protic or aprotic solvents, a water–organic mixture, biphasic solvents, and ionic liquids, have been evaluated for hexose dehydration.<sup>[15a–g]</sup> The solvent composition plays an important role in controlling the rate and selectivity of hexose dehydration by influencing the solubility of hexose, tautomer distribution of hexose, stability of intermediates and/or products, and the forms of active species.<sup>[16a–f]</sup> In particular, the tautomer distribution of hexose in solvents primarily controls HMF selectivity.<sup>[17a–c]</sup> For D-fructose, five tautomers (i.e.,  $\alpha$ -D-fructofuranose ( $\alpha$ -furanose),  $\beta$ -D-fructofuranose ( $\beta$ -furanose),  $\alpha$ -D-fructopyranose ( $\alpha$ -pyranose),  $\beta$ -D-fructopyranose ( $\beta$ -pyranose), and acyclic keto D-fructose (open-chain)) are included in solution (Scheme 2).<sup>[18a,b]</sup> At 120 °C, fructose predominantly exists as  $\beta$ -furanose (39%) and  $\beta$ -pyranose (37%) in H<sub>2</sub>O, but mainly  $\beta$ -furanose (46%) and  $\alpha$ -furanose (25%) in DMSO.<sup>[19]</sup> Notably, the dominant existence of fructofuranose tautomer in DMSO was proposed to lead to HMF, whereas the fructopyranose form in water led to oligo-



**Scheme 2.** Structures of five tautomers of fructose and their interconversion via open-chain fructose.

mers.<sup>[20a–c]</sup> However, to the best of our knowledge, little effort has been made to demonstrate the intrinsic solvent effect on the degradative condensation of fructose, especially the relationship between the tautomeric distribution of fructose and the formation of humins at the initial reaction stage in various solvents. The lack of this fundamental understanding hampers guidance for the design of optimal reaction systems for inhibiting humin formation in HMF production.

Herein, the impact of several typical polar aprotic solvents [i.e., 1,4-dioxane (DIO), THF, 4-methyl-2-pentanone (MIBK),  $\gamma$ -valerolactone (GVL), *N*-methylpyrrolidone (NMP), and dimethyl sulfoxide (DMSO)] on the side reactions of fructose to small-molecule carboxylic acids and oligomers (the possible precursors of humins) through degradative condensation in the initial stage of fructose conversion is studied. The solvents are chosen based on their frequent applications in acid-catalyzed fructose-to-HMF dehydration. The product distributions in the presence or absence of acid catalyst in various solvents reveal the popular formation of FA and oligomers through degradative condensation in DIO or THF, acetic acid (AA) and oligomers in MIBK, LA and oligomers in GVL or NMP, and HMF in DMSO. The intrinsic solvent effect on different product distributions has been probed by performing fructose conversion in the absence of an acid catalyst to approach an earlier reaction stage and exclude the influence of HMF formed. In situ attenuated total reflection-infrared spectroscopy (ATR-IR), electrospray ionization mass spectrometry (ESI-MS/MS), and quantum chemical calculations have been used to investigate the mutual evolution of each fructose tautomer, the predominant tautomer, and the correlation between the tautomeric distribution of fructose and the mechanism of degradative condensation in various solvents.

## Results and Discussion

### Effect of solvents on the product distribution in the initial stage of fructose conversion

In the presence of HCl, a Brønsted acid catalyst, fructose (250.0 mM) underwent fast dehydration to HMF within 2 min (even 20 s) at 120 °C in various solvents (Table S1 in the Supporting Information); thus indicating that the solvents were all suitable for fructose-to-HMF dehydration.<sup>[21]</sup> Additionally, we observed the predominant formation of FA in DIO or THF, AA in MIBK, and LA in GVL or NMP within 20 s of reaction. These small-molecule carboxylic acids were clearly the products from the direct degradation of fructose. However, no C<sub>5</sub> or smaller products were detected in DIO or THF to accompany the formation of FA, no C<sub>4</sub> or smaller products were detected in MIBK to accompany the formation of AA, and only a stoichiometrically smaller amount of FA was detected with the formation of LA in GVL or NMP. These results suggested that the degraded fructose fragments might have undergone further transformation, typically a condensation reaction, to form products that could not be detected by means of HPLC. Within such a short reaction time of 20 s or 2 min, no insoluble humins were observed in any solvents, thereby demonstrating the possible for-

**Table 1.** Effect of solvents on the conversion of fructose in the initial reaction stage.<sup>[a]</sup>

Entry	Solvent	Fru conversion [mol%]	Yield [mol%]				Carbon balance [mol%]		
			HMF	FA	AA	LA	actual	theoretical <sup>[b]</sup>	difference <sup>[c]</sup>
1	DIO	43.3 (17.0)	– (–)	27.2 (46.2)	– (–)	– (–)	61.2 (90.7)	83.9 (98.4)	22.7 (7.7)
2	THF	27.0 (25.8)	– (–)	3.0 (14.9)	– (–)	– (–)	73.5 (76.7)	76.0 (89.1)	2.5 (12.4)
3	MIBK	58.3 (26.8)	– (–)	0.1 (–)	10.7 (18.2)	– (–)	45.3 (79.3)	52.5 (91.4)	7.2 (12.1)
4	GVL	27.3 (33.7)	– (–)	0.3 (–)	– (–)	19.9 (31.7)	89.3 (82.9)	92.9 (86.2)	3.6 (3.3)
5	NMP	15.5 (29.7)	– (–)	0.3 (–)	– (–)	13.7 (23.4)	96.0 (81.7)	98.5 (84.0)	2.5 (2.3)
6	DMSO	68.1 (16.2)	38.7 (0.1)	– (–)	– (–)	– (–)	70.6 (83.9)	70.6 (83.9)	– (–)

[a] Reaction conditions: 250.0 mm fructose, solvent (1 mL), 120 °C, 1 h. The values in parentheses represent data obtained by reacting 27.8 mm fructose for 30 min. [b] The theoretical carbon balance was estimated by assuming that the lost carbon merely came from the degradative condensation of fructose.

[c] The difference between the theoretical and actual values, which represents the lost percentage of carbon owing to the degradation of fructose.

mation of oligomers through degradation and subsequent condensation in the initial stage of fructose dehydration. Actually, the promotional solvent effect of THF on the formation of FA and oligomers was in accordance with our previous study, wherein a Lewis or Brønsted acid was added for fructose dehydration.<sup>[12,22]</sup> Notably, the conversion of fructose (250.0 mm) in the absence of acid catalyst at 120 °C for 1 h resulted in the same product distributions as those in the presence of HCl catalyst. The results are shown in Table 1, wherein FA was found to be the sole product in DIO or THF (entries 1 and 2), AA was the predominant product in MIBK (entry 3), LA was the predominant product in GVL or NMP (entry 4 and 5), and HMF was the only product in DMSO (entry 6). Herein, the formation of HMF in DMSO originated from the well-known catalytic performance of DMSO.<sup>[16a,23]</sup> On account of the above results, the formation of small-molecule carboxylic acids (i.e., FA, AA, and/or LA) could be considered as an important message for predicating the formation of oligomers in the initial stage of fructose dehydration. Moreover, the theoretical carbon balance was clearly higher than that of the actual carbon balances in DIO, THF, MIBK, GVL, or NMP, which suggested the occurrence of the degradative condensation of fructose in the initial reaction stage of fructose conversion without adding acid catalyst. Therefore, the occurrence of degradative condensation of fructose is a popular reaction pathway in various polar aprotic solvents in either the presence or absence of acid catalyst; thus indicating the intrinsic influence of the solvents used on the formation of small-molecule carboxylic acids and oligomers in the initial reaction stage of fructose conversion. To probe this intrinsic solvent effect, the fructose conversions in the subsequent study were all conducted by reacting fructose in the absence of any catalyst.

Considering the fact that some fructose remained undissolved in THF, MIBK, or GVL owing to the solubility limit, we further lowered the initial fructose concentration to 27.8 mm to ensure complete dissolution and decreased the reaction time from 1 h to 30 min to approach an earlier reaction stage. The results are also shown in Table 1. Notably, the reduction of fructose concentration and reaction time led to the same product distribution of small-molecule carboxylic acids in a given polar aprotic organic solvent, which strongly illustrated that the fructose solubility and undissolved fructose had little influence on determining the product evolutions in the initial reac-

tion stage of fructose conversion. Furthermore, the time profiles within 1 h (Figure S1 in the Supporting Information)<sup>[21]</sup> illustrated the increase of FA yield in DIO, the predominant increase of AA yield in MIBK, and the predominant increase of LA in NMP. In other words, fructose conversion in a given solvent within 1 h gave out the same product distribution, which was not affected by the reaction time or the fructose concentration in the initial stage of fructose conversion. Although the polarity of solvents has been reported to influence the product distributions during hexose conversion,<sup>[16c]</sup> no correlation between the solvent polarity (order: MIBK > NMP > GVL > DIO > DMSO > THF) and the formation of carboxylic acids could be established. Additionally, the possible influence of the actual reaction pressures on the degradative condensation of fructose were excluded because the similarly higher reaction pressures (0.26–0.38 MPa) in DIO, THF, or MIBK led to different carboxylic acids (i.e., FA or AA), and the same reaction pressure (0.18 MPa) in NMP and DMSO also resulted in different products (i.e., LA or HMF; Table S2 in the Supporting Information).<sup>[21]</sup> The possible decomposition of FA into CO<sub>2</sub>, CO, or H<sub>2</sub> under the reaction conditions was also excluded by analyzing the gaseous products with GC coupled to a thermal conductivity detector (TCD), which made the quantification of FA reliable.

### Effect of solvents on the possible structure of oligomers

The formation of oligomers was the main factor for carbon loss during fructose conversion. To explore possible structures of oligomers originally derived from the degradative condensation of fructose in the initial stage of fructose conversion, the reaction mixtures, after reacting fructose at 120 °C for 1 h in various solvents, were analyzed by means of ESI-MS/MS (Figure 1). The results showed the formation of two kinds of dimerized products in the initial reaction stage: 1) dimers with *m/z* 365, 347, 311, 293, or 275 in all of the solvents were assigned to [2Fru-*n*H<sub>2</sub>O+Na]<sup>+</sup> (*n*=1–6) species that formed through intermolecular etherification of fructose and subsequent dehydration; and 2) dimers with *m/z* 305 and 247 in DIO, 273 in THF, 301–368 in MIBK, 319 and 223 in GVL, and 221 in NMP were assigned to the dimerized products through the degradation of fructose and further dimerization of degraded fructose fragment with another fructose molecule. For

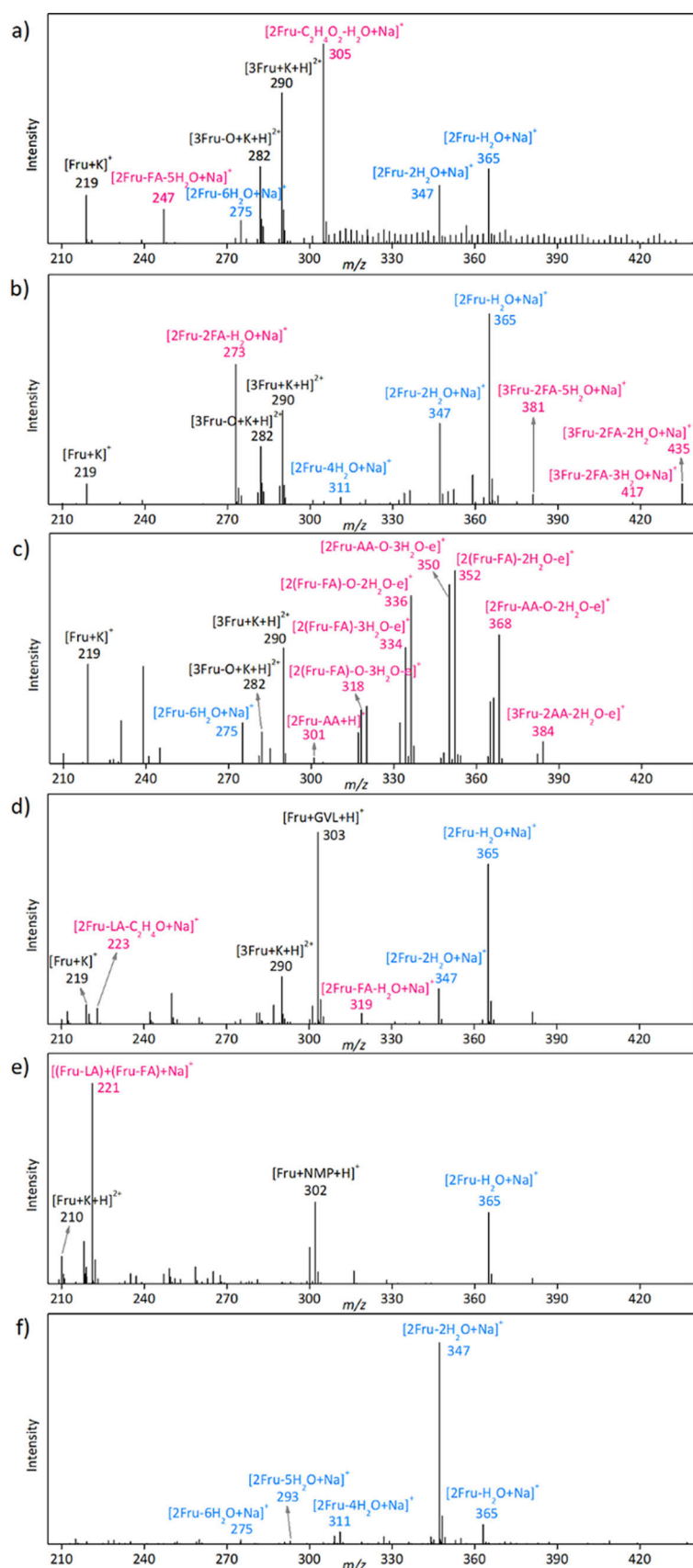
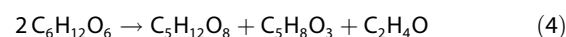
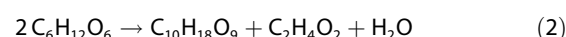
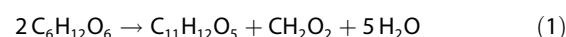


**Figure 1.** ESI-MS spectra of reaction mixtures after reacting fructose (Fru) in various solvents at 120 °C for 1 h. a) DIO, b) THF, c) MIBK, d) GVL, e) NMP, and f) DMSO.

instance, the species with  $m/z$  247 was assigned to  $[2\text{Fru-FA-5H}_2\text{O} + \text{Na}]^+$  (i.e.,  $[\text{C}_{11}\text{H}_{12}\text{O}_5 + \text{Na}]^+$ ), the species with  $m/z$  305 was assigned to  $[2\text{Fru-C}_2\text{H}_4\text{O}_2\text{-H}_2\text{O} + \text{Na}]^+$  (i.e.,  $[\text{C}_{10}\text{H}_{18}\text{O}_9 + \text{Na}]^+$ , as verified by ESI-MS/MS results in Figure S2 in the Supporting Information),<sup>[21]</sup> the species with  $m/z$  273 was assigned to  $[2\text{Fru-2FA-H}_2\text{O} + \text{Na}]^+$  (i.e.,  $[\text{C}_{10}\text{H}_{18}\text{O}_7 + \text{Na}]^+$ ), the species with  $m/z$  223 was assigned to  $[2\text{Fru-LA-C}_2\text{H}_4\text{O}_2 + \text{Na}]^+$  (i.e.,  $[\text{C}_5\text{H}_{12}\text{O}_8 + \text{Na}]^+$ ), and the species with  $m/z$  221 was assigned to  $[2\text{Fru-LA-FA} + \text{Na}]^+$  (i.e.,  $[\text{C}_6\text{H}_{14}\text{O}_7 + \text{Na}]^+$ ), according to Equations (1)–(5):



However, at room temperature, the etherized dimers were only observed in DMSO or NMP, whereas the dimerized products formed through the degradative condensation of fructose were not observed at all in any solvents. Therefore, the different appearance of etherized or degradative-condensed oligomers in a given solvent was induced by the high-temperature reaction, rather than the ESI or solvent themselves.

Also, the possible molecular formula of the oligomers revealed the release of small-molecule carboxylic acids during the degradative condensation of fructose. Typically, one molecular glycolaldehyde (or its isomer) was released from fructose in DIO (Figure 1a); however, no glycolaldehyde (or its isomer) was detected in the time profile of fructose conversion in this solvent (Figure S1a in the Supporting Information).<sup>[21]</sup> This result was possibly ascribed to the unstable characteristics of glycolaldehyde (or its isomer) in the reaction system.<sup>[24a,b]</sup> Once formed, glycolaldehyde (or its isomer) might immediately decompose to generate FA as the final product detected. Whereas, in THF, only the FA-related dimers (e.g.,  $[2\text{Fru-2FA-H}_2\text{O} + \text{Na}]^+$ ) were detected in the ESI-MS spectrum (Figure 1b), which was indicative of the release of FA during the degradative dimerization of fructose in THF. Therefore, although FA was detected as the product in both DIO and THF, the different structures of dimers were indicative of the different evolution routes of FA in these two typical aprotic solvents containing similar epoxy structures. Meanwhile, we also observed the formation of some trimerized products in THF. For instance, the species with  $m/z$  381 was assigned to  $[3\text{Fru-2FA-5H}_2\text{O} + \text{Na}]^+$ , the species with  $m/z$  417 was assigned to  $[3\text{Fru-2FA-3H}_2\text{O} + \text{Na}]^+$ , and the species with  $m/z$  435 was assigned to  $[3\text{Fru-2FA-2H}_2\text{O} + \text{Na}]^+$ . The

observation of trimerized products in THF provided a clue to the formation of trimers by further condensation reactions.

Similarly, the ESI-MS spectra of the products after reacting fructose in MIBK, GVL, and NMP also illustrated the formation of oligomers derived from the degradative condensation of fructose, for which the signals at  $m/z$  301 to 384 were mainly ascribed to the di- or trimerized species after releasing AA or FA molecules from fructose in MIBK (Figure 1 c), the signals at  $m/z$  223 and 319 were assigned to dimerized species  $[2\text{Fru-LA-C}_2\text{H}_4\text{O} + \text{Na}]^+$  and  $[2\text{Fru-FA-H}_2\text{O} + \text{Na}]^+$  after releasing LA or FA molecules from fructose in GVL (Figure 1 d), and the signal at  $m/z$  221 corresponded to  $[2\text{Fru-LA-FA} + \text{Na}]^+$  derived from the condensation of degraded fructose fragment after the release of FA or LA in NMP (Figure 1 e). Additionally, the appearance of signals assigned to  $[\text{Fru} + \text{GVL} + \text{Na}]^+$  ( $m/z$  303; Figure 1 d) and  $[\text{Fru} + \text{NMP} + \text{Na}]^+$  ( $m/z$  302; Figure 1 e) was explained by the possible aggregation of charged ions between fructose and solvent molecules after ionization.<sup>[25]</sup> Notably, no signals assigned to the products from the degradative condensation of fructose were observed in DMSO (Figure 1 f). Instead, the appearance of signals corresponding to  $[2\text{Fru-}n\text{H}_2\text{O} + \text{Na}]^+$  ( $n = 1-6$ ) species supported the mechanism of difructose anhydride (DFA)-mediated fructose-to-HMF dehydration in DMSO because of the highly stable existence of caramel-like<sup>[26]</sup>  $[2\text{Fru-}2\text{H}_2\text{O} + \text{Na}]^+$  ( $m/z$  347) species.<sup>[17b,27a,b]</sup> However, it is interesting to note that the  $[2\text{Fru-H}_2\text{O} + \text{Na}]^+$  ( $m/z$  365) species was found to be the main DFA species in DIO, THF, GVL, and NMP. The different existence forms of the DFAs in various solvents might be indicative of different conversion paths of fructose at the initial reaction stage, which deserves a deeper study in our future work.

Significantly, we have also detected the formation of oligomers as tetra-, penta-, hexa-, hepta-, and nonamers in the ESI/MS spectra of the reaction mixture after reacting fructose in the presence of HCl in various solvents (Figure S3 in the Supporting Information).<sup>[21]</sup> Therefore, the di- and trimers formed in the initial reaction stage of fructose conversion were supposed to act as "precursors" or "cores" to trigger subsequent oligomerization, typically cross-condensation with HMF or other highly active intermediates during acid-catalyzed fructose dehydration. Considering this point, suppression of the degradative condensation pathway in the initial reaction stage of fructose dehydration is of particular importance to inhibit the formation of humins.

### In situ ATR-IR spectra for the initial fructose conversion in typical solvents

To probe the effects of solvent on the formation of oligomers through degradative condensation in the initial stage of fructose conversion, the in situ ATR-IR spectra of the reaction mixtures during fructose conversion at 120 °C were monitored. The raw spectra are shown in Figure S4 in the Supporting Information,<sup>[21]</sup> whereas the spectra after deducting the solvent bands to exclude solvent disturbance are exhibited in Figure 2a and c and Figure S5a–S8a in the Supporting Information.<sup>[21]</sup> To assist recognizing the tautomers of fructose in the

solvents, theoretical calculations of the IR spectra of each tautomer were performed by using Gaussian 09 software at the B3LYP/6-31+G(d,p) level of theory. Considering the overlapping of IR signals between  $\alpha$ - and  $\beta$ -configured tautomers, only the characteristic IR bands attributed to  $\beta$ -furanose,  $\beta$ -pyranose, and open-chain fructose are shown in Table S3 in the Supporting Information.<sup>[21]</sup> Because of the exclusive attribution, the IR band at 778  $\text{cm}^{-1}$ , which was assigned to the vibration of  $\text{C}_1\text{-O-H}$  in open-chain fructose, and 1084  $\text{cm}^{-1}$  which was assigned to the vibrations of  $\text{C}_4\text{-C}_5$ ,  $\text{C}_5\text{-O-H}$ , and  $\text{C}_1\text{-O-H}$  in pyranose, could be used to represent the characteristic signals of open-chain fructose and fructopyranose, respectively. Although the band at 1725  $\text{cm}^{-1}$ , which was assigned to the  $\text{C=O}$  stretching vibration, was also a characteristic IR band for open-chain fructose,<sup>[28]</sup> it was not an ideal characteristic signal on account of its overlap with the IR bands of solvents (i.e., MIBK, GVL, or NMP) that contained a  $\text{C=O}$  group.

The variations of the intensity of bands at 778 ( $I_{778}$ ) and 1084  $\text{cm}^{-1}$  ( $I_{1084}$ ) in various solvents are plotted in Figure 2b and d and Figure S5b–S8b in the Supporting Information,<sup>[21]</sup> wherein the increase of the intensity of the band at an earlier stage was indicative of the dissolution of fructose because fructofuranose (crystalline fructose) in solvent would be transferred into fructopyranose via open-chain fructose to reach an equilibrium tautomer distribution. After complete dissolution, the intensity variations in the curves would further imply configuration changes during the tautomerization process. From the in situ ATR-IR spectra, we observed different dissolution and tautomerization times for fructose in different solvents (Table S4 in the Supporting Information).<sup>[21]</sup> Fructose dissolved quickly in GVL (15 min), NMP (5 min), or DMSO (3 min), but slowly in DIO (30 min), THF (50 min), or MIBK (30 min). Meanwhile, faster dissolution favored a faster tautomerization equilibrium. It was noted that a longer dissolution time ( $\geq 30$  min) in DIO, THF, or MIBK favored the formation of shorter-chain carboxylic acids (i.e., FA or AA) and oligomers, but the shorter dissolution times ( $\leq 15$  min) in GVL, NMP, or DMSO favored the formation of longer-chain products (i.e., LA or HMF) with or without oligomers. Nevertheless, the same dissolution times in DIO and MIBK led to different products (FA vs. AA), and the same tautomerization equilibrium times in GVL and DMSO also led to different products (LA vs. HMF), thereby indicating that the time for dissolution and tautomerization equilibrium was not the key factor that determined product evolution in the initial stage of fructose conversion.

Notably, we found that the formation of a special initial product to accompany oligomers was related to the main fructose tautomer existing in a given solvent during both the dissolution and tautomerization processes. In DIO (Figure 2b), the faster increase of  $I_{778}$  than that of  $I_{1084}$  was indicative of the faster formation of open-chain fructose and slower formation of fructopyranose, thereby revealing the main existence of fructofuranose or open-chain fructose in DIO during the dissolution stage. After dissolution, the decrease of  $I_{778}$  illustrated the gradual decrease of the open-chain fructose tautomer and the nearly unchanged  $I_{1084}$  suggested a balanced content of pyranose tautomer after fructose dissolution. Therefore, it was

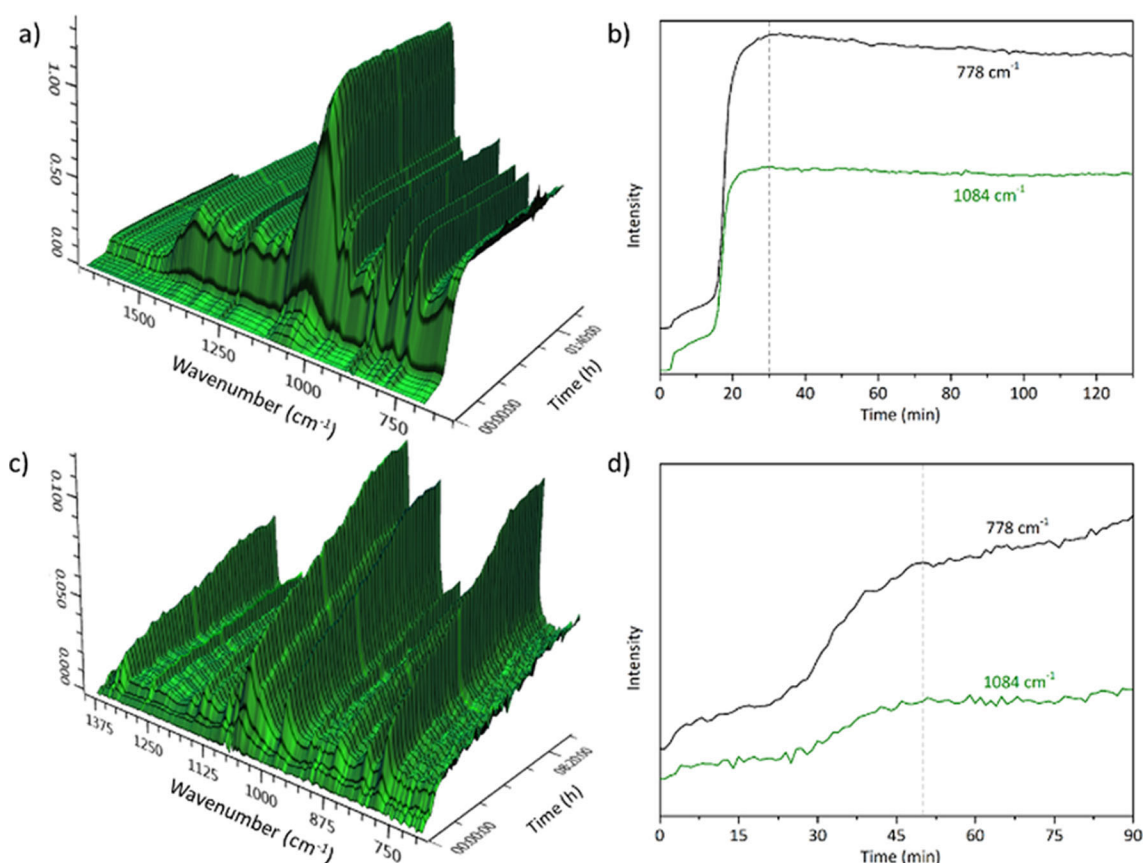


**Figure 2.** In situ ATR-IR spectra of the reaction mixture during fructose conversion at 120 °C in a) DIO and c) THF. b) and d) Intensity variation of selected characteristic bands [ $\nu = 778 \text{ cm}^{-1}$ :  $\delta(\text{C}_1\text{--O--H})$  in open-chain fructose;  $\nu = 1084 \text{ cm}^{-1}$ :  $\nu(\text{C}_4\text{--C}_5)$ ,  $\delta(\text{C}_5\text{--O--H})$ , and  $\delta(\text{C}_1\text{--O--H})$  in pyranose]. The dashed line signifies the time for complete dissolution of fructose in the solvent. Reaction conditions: fructose (55.6 mmol), solvent (50 mL), 120 °C.

reasonable to deduce that the content of furanose tautomer increased during the tautomerization process. Accordingly, the combination of increasing furanose tautomer and increasing FA yield with increasing reaction time in DIO revealed the main contribution of fructofuranose to the formation of FA and oligomers in the initial fructose conversion in DIO. In THF (Figure 2d),  $I_{778}$  and  $I_{1084}$  showed similar increases to that in DIO during the gradual dissolution process, thereby supporting the chain opening of fructose during dissolution. After dissolution,  $I_{778}$  kept increasing, whereas  $I_{1084}$  remained unchanged; this was indicative of the stable existence of open-chain fructose in THF during tautomerization. Therefore, the combination of increasing open-chain fructose tautomer and increasing FA yield with increasing reaction time in THF demonstrated the main contribution of open-chain fructose to the formation of FA and oligomers during initial fructose conversion in THF. The existence of different tautomers in DIO and THF might be used to explain the different evolution routes of FA, accompanying the generation of different kinds of soluble humins (see above). In a similar way, we found that fructose existed mainly in the fructopyranose form in MIBK or GVL, but mainly in the fructofuranose form in NMP or DMSO. Therefore, a correlation between the predominant form of tautomers and product evolutions in the initial stage of fructose conversion might be obtained (see below).

#### Quantum chemical calculations on tautomer distribution of fructose in the solvents

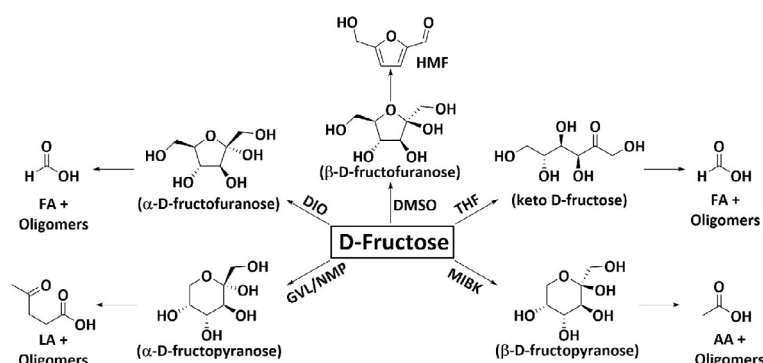
To simulate the real solvent environment and actual solvent effect on the tautomeric distribution of fructose, we performed quantum chemical calculations at the pbepbe/maug-cc-pvdz level of theory with implicit solvation in the polarizable continuum model (PCM) by using Gaussian 09 software. The hydrogen-bonding interactions between the tautomers of fructose and solvent molecules were investigated, wherein six solvent molecules were added to each tautomer to saturate the hydrogen bonding of fructose and two forms of open-chain fructose (open-chain I and open-chain II) were used to increase the amount of sample (Figure S9 in the Supporting Information).<sup>[21]</sup> The sum of electronic and thermal Gibbs free energies of the simulated tautomers in the solvents are shown in Tables S5–S10 in the Supporting Information,<sup>[21]</sup> and the relative Gibbs free energies of the simulated tautomers are calibrated by setting the Gibbs free energy of  $\beta$ -furanose tautomer to zero. From the results shown in Table 2, we found that  $\alpha$ -furanose had the lowest Gibbs free energy in DIO (entry 1) and open-chain fructose had the lowest Gibbs free energy in THF (entry 2). In other words,  $\alpha$ -furanose was the dominant tautomer in DIO and open-chain fructose was the dominant tautomer in THF, which was consistent with the results from in situ

**Table 2.** Relative Gibbs free energies of different tautomers of fructose in various solvents at 120 °C.<sup>[a]</sup>

Entry	Solvent	Relative Gibbs free energies [kJ mol <sup>-1</sup> ]					
		$\alpha$ -furanose	$\beta$ -furanose	$\alpha$ -pyranose	$\beta$ -pyranose	open-chain I	open-chain II
1	DIO	-12.3	0.0	5.5	-5.3	12.9	-3.4
2	THF	-10.7	0.0	-4.8	-2.7	-22.4	-7.2
3	MIBK	-13.2	0.0	-6.1	-15.6	-1.8	-10.3
4	GVL	-9.6	0.0	-20.5	0.3	-7.9	-16.2
5	NMP	-10.8	0.0	-6.0	3.9	9.2	9.2
6	DMSO	16.4	0.0	1.1	13.4	26.5	12.4

[a] The relative Gibbs free energies of the simulated tautomer were calibrated by setting the Gibbs free energy of  $\beta$ -furanose tautomer to zero.

ATR-IR spectra (see above). Moreover,  $\beta$ -pyranose was the dominant tautomer in MIBK, with  $\alpha$ -furanose in second place with a small  $\Delta G$  of 2.4 kJ mol<sup>-1</sup> (Table 2, entry 3). In GVL, the dominant tautomeric configuration of fructose was  $\alpha$ -pyranose with open-chain II as the second most popular configuration ( $\Delta G = 4.3$  kJ mol<sup>-1</sup>; Table 2, entry 4). In NMP,  $\alpha$ -furanose existed as the dominant tautomer, with  $\alpha$ -pyranose in second place ( $\Delta G = 4.8$  kJ mol<sup>-1</sup>; Table 2, entry 5). As expected,  $\beta$ -furanose had the lowest energy configuration in DMSO (Table 2, entry 6), which would favor the dehydration pathway that led to HMF formation. The combination of in situ ATR-IR spectra and quantum chemical computations revealed that the formation of oligomers through degradative condensation in the initial stage of fructose conversion in a given solvent was closely related to the type of predominant fructose tautomer. The relationships between the dominant tautomer distribution of fructose in solvents and the formation of small-molecule products and oligomers in various solvents are shown in Scheme 3,



**Scheme 3.** The relationship between the dominant tautomer distribution of fructose in solvents and the formation of small-molecule products and oligomers.

wherein  $\alpha$ -fructofuranose in DIO and acyclic open-chain fructose in THF favor the degradative condensation of fructose to FA and oligomers,  $\alpha$ -fructopyranose in GVL or NMP favors the degradative condensation of fructose to LA and oligomers, and  $\beta$ -fructopyranose in MIBK favors the degradative condensation of fructose to AA and oligomers.

### Solvent effects on the degradative condensation of fructose to small-molecule carboxylic acids and concomitant oligomers

As shown in Figure 3, a deliberate analysis of the geometric structures of fructose tautomers before and after solvation provided information on the effects of solvent on the interaction between fructose and solvent molecules and its influence on fructose conversion. The variations of bond lengths in C–C and C–O in each tautomer are summarized in Tables S11 and S12 in the Supporting Information,<sup>[21]</sup> respectively. In DIO, a clear elongation of the C<sub>3</sub>–C<sub>4</sub> and C<sub>4</sub>–C<sub>5</sub> bonds of  $\alpha$ -furanose was observed, whereas the length of the C–O bond was decreased or remained unchanged. This variation in bond length was supposed to result in the final cleavage of C<sub>5</sub>–C<sub>6</sub> or C<sub>4</sub>–C<sub>5</sub> bonds of  $\alpha$ -furanose to generate FA directly (Figure 4a) or indirectly (Figure 4b). In the direct route, C<sub>5</sub>–C<sub>6</sub> bond cleavage of  $\alpha$ -furanose underwent a decarboxylation mechanism,<sup>[20b]</sup> producing FA directly. In the indirect route, C<sub>4</sub>–C<sub>5</sub> bond cleavage of  $\alpha$ -furanose underwent a retro-aldol condensation mechanism,<sup>[29]</sup> producing glycolaldehyde (or its isomer) followed by further decomposition to FA, according to reports in the literature.<sup>[16b,21,24b,30]</sup> During both evolution processes, oligomers would form as the result of further condensation of unstable degraded fragments with fructose. In THF, the elongation of C<sub>1</sub>–C<sub>2</sub> and C<sub>4</sub>–C<sub>5</sub> bonds in open-chain I fructose was more prominent, whereas the length of C–O bonds decreased or remained constant, which was proposed to result in cleavage of the C<sub>1</sub>–C<sub>2</sub> bond in open-chain I fructose to form FA and oligomers in the initial stage of fructose conversion (Figure 4c). In other words, the unstable deoxypentose intermediates formed through fructose degradation in THF would undergo further condensation to form di- (*m/z* 273) or trimers (*m/z* 381/417/435), and then be further polymerized to a hexamer (*m/z* 851) with a higher degree of polymerization. Whereas, in MIBK, AA was conceivably generated from C<sub>2</sub>–C<sub>3</sub> cleavage of  $\beta$ -pyranose owing to the simultaneous increase in lengths of C<sub>2</sub>–C<sub>3</sub> and C<sub>2</sub>–O<sub>R</sub> (O<sub>R</sub>: the epoxy oxygen) bonds after solvation, minor formation of FA originated from C<sub>5</sub>–C<sub>6</sub> cleavage of  $\alpha$ -furanose (Figure S10 in the Supporting Information).<sup>[21]</sup> In GVL, LA might come from C<sub>1</sub>–C<sub>2</sub> cleavage of  $\alpha$ -pyranose, whereas the minor product of FA ori-

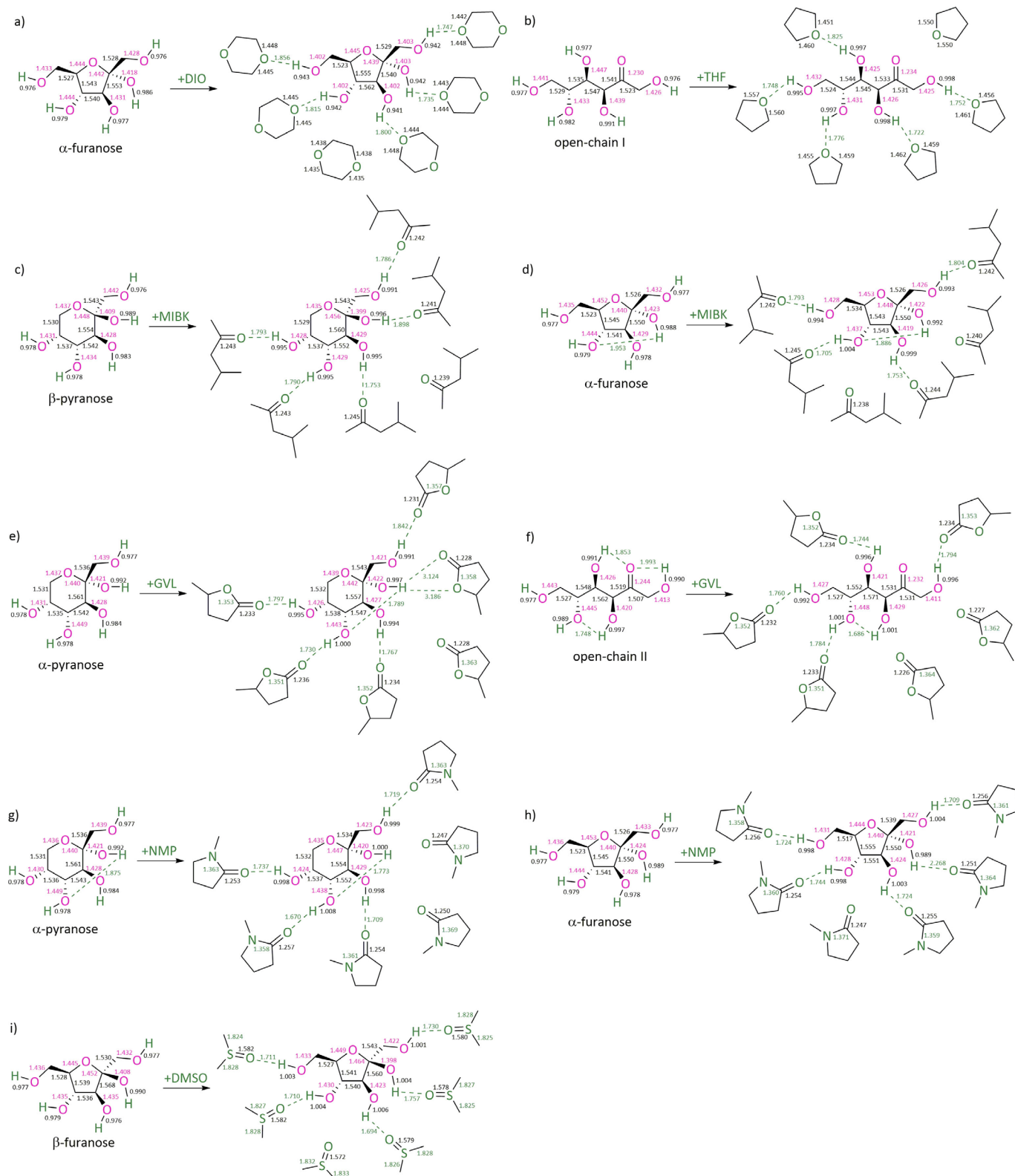


**Figure 3.** Structures of fructose tautomers and solvated tautomers. Possible hydrogen bonding between the hydroxyl of fructose and oxygen of each solvent is indicated by dotted lines. The digits represent the lengths of corresponding C–C, C–O, or O–H bonds.

ginated from C<sub>1</sub>–C<sub>2</sub> cleavage of open-chain II fructose (Figure S11 in the Supporting Information).<sup>[21]</sup> In NMP, LA was deemed to be the product of C<sub>1</sub>–C<sub>2</sub> cleavage of  $\alpha$ -pyranose

and FA came from C<sub>1</sub>–C<sub>2</sub> cleavage of  $\alpha$ -furanose (Figure S12 in the Supporting Information).<sup>[21]</sup> According to reports in the literature,<sup>[16a]</sup> in DMSO, the elongation of both C<sub>1</sub>–C<sub>2</sub> and C<sub>2</sub>–O<sub>R</sub>

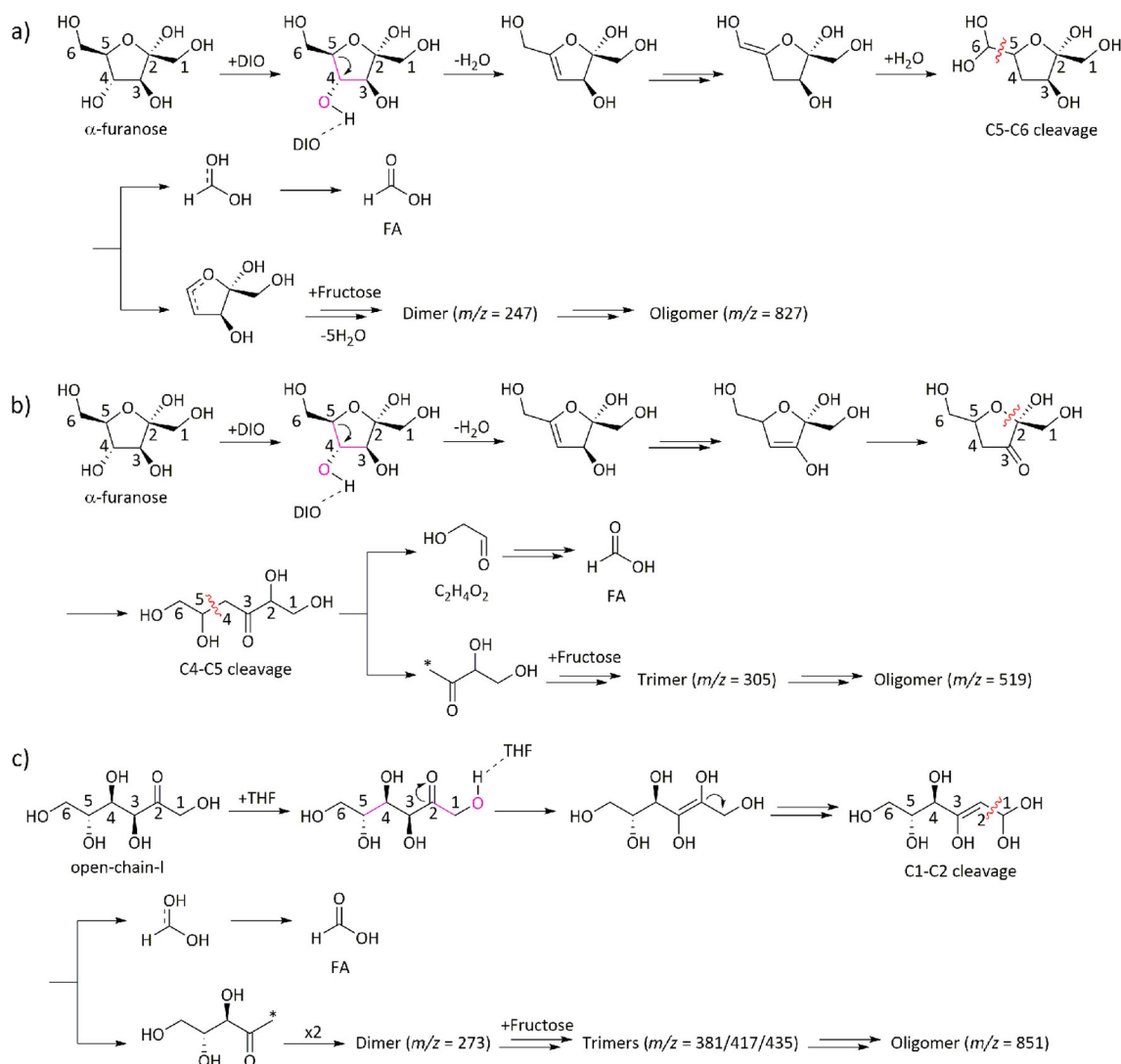


**Figure 4.** Three possible reaction pathways for transforming  $\alpha$ -fructofuranose or open-chain fructose into FA and oligomers in DIO or THF. The elongated C–C bond is indicated in red.

bonds after solvation led to the successive dehydration of  $\beta$ -fructofuranose to form HMF as the product (Figure S13 in the Supporting Information).<sup>[21]</sup> From these results, we reasonably infer that the existence of  $\alpha$ -fructofuranose in solvents such as DIO, MIBK, or NMP results in a pathway toward FA formation directly from fructose. Meanwhile, the existence of acyclic open-chain fructose in solvents such as THF or GVL also accounts for initial FA formation. Alternatively, the dominant existence of  $\alpha$ -fructopyranose in GVL or NMP leads to a popular pathway toward LA formation directly from fructose. Moreover, the dominant existence of  $\beta$ -fructopyranose in MIBK favors the pathway toward AA formation. All of these processes generate oligomers as the side products during fructose-to-HMF dehydration. Notably, the dominant existence of  $\beta$ -fructofuranose in DMSO contributes to favorable fructose-to-HMF dehydration, wherein degradative condensation is inhibited as much as possible.

From the above discussion, we have demonstrated that the solvent plays an important role in controlling the formation of

small molecules and oligomers by affecting the dissolution of fructose and dominant existence of tautomers of fructose, even in the initial reaction stage. Once formed, these oligomers might be transformed into insoluble ones through further condensation with HMF, as we have detected in solvents containing a Brønsted acid catalyst. Clearly, an unsuitable selection of solvent for hexose dehydration will result in the conspicuous formation of humins and carbon losses, which disfavor the effective utilization of biomass-derived carbons for HMF production. Therefore, the cautious selection of solvent needs to be preferentially considered in designing an effective catalytic system for HMF production in the future.

## Conclusions

We reported the effects of solvent on the degradative condensation of fructose in the initial stage of fructose conversion, wherein 1,4-dioxane (DIO), THF, 4-methyl-2-pentanone (MIBK),  $\gamma$ -valerolactone (GVL), *N*-methylpyrrolidone (NMP), and dimeth-

yl sulfoxide (DMSO) were used as typical polar aprotic solvents. Significant amounts of small-molecule carboxylic acids [i.e., formic acid (FA), acetic acid (AA), and levulinic acid (LA)] have been detected as the degraded products associated with the formation of oligomers, which are the possible precursors or cores of insoluble humins. We showed the dominant formation of FA and oligomers in DIO or THF, AA and oligomers in MIBK, LA and oligomers in GVL or NMP, and HMF in DMSO in the initial stage of fructose conversion. Different product distributions in various solvents have been ascribed to the dominant existence of specific tautomers of fructose governed by solvents, as revealed by in situ attenuated total reflection-infrared spectroscopy (ATR-IR), electrospray ionization mass spectrometry (ESI-MS), and quantum chemical calculations. In other words,  $\alpha$ -fructofuranose in DIO and acyclic open-chain fructose in THF favor the degradative condensation of fructose to form FA and oligomers,  $\alpha$ -fructopyranose in GVL or NMP leads to degradative condensation to LA and oligomers,  $\beta$ -fructopyranose in MIBK benefits degradative condensation to AA and oligomers, and  $\beta$ -fructofuranose in DMSO contributes to fructose-to-HMF dehydration. The formation mechanism of small-molecule carboxylic acids and concomitant oligomers have been proposed. This close relationship between the dominant tautomer distribution of fructose in various solvents and the formation of oligomers at the initial stage of fructose conversion provide a universal understanding of the solvent-controlled formation of humins in the initial stage of fructose dehydration, which represents an important step towards the rational design of effective solvent systems for HMF production.

## Experimental Section

### Materials

Analytical reagent (A.R.) grade fructose was purchased from TCI Reagent Factory. All other chemicals of A.R. grade were purchased from J&K Scientific Ltd. Water, used in all experiments, was ultra-pure ( $18.25 \text{ m}\Omega \text{ cm}^{-1}$ ). All chemicals were used as received.

### Conversion of fructose in various aprotic solvents

All reactions were performed in a thick-walled pressured tube (Synthware Corporation, 15 mL), wherein the reaction temperature was controlled by an automatic temperature controller. In a typical synthetic experiment, fructose (0.25 or 0.0278 mmol) and solvent (1 mL) were mixed in the reaction tube, followed by being sealed and placed in an oil bath already heated at  $120^\circ\text{C}$  under continuous stirring (400 rpm). The required reaction time (1 h or 30 min) was counted once the reaction temperature reached  $120^\circ\text{C}$ . After the reaction, the tube was removed from the oil bath and cooled to room temperature gradually. For the HCl-catalyzed conversion of fructose, HCl (0.075 mmol) was added as the catalyst, while other reaction conditions, except reaction time, were unchanged. To investigate the initial product evolution, the reaction time of HCl-catalyzed fructose conversions was controlled to be 20 s.

### Product analysis

Quantitative analysis of the liquid products was performed by means of HPLC (Dionex U-3000, Thermo Fisher Scientific) by using an aminex column (Model HPX-87 H, 300 mm  $\times$  7.8 mm, Bio-Rad), a variable-wavelength detector (Model VWD-3  $\times$  00(RS)), and a refractive index (RI) detector (Model RI-101, Shodex). A solution of  $\text{H}_2\text{SO}_4$  ( $5 \text{ mmol L}^{-1}$ ) was used as the mobile phase at a flow rate of  $0.6 \text{ mL min}^{-1}$ . The temperatures of the column and RI detector were maintained at 50 and  $35^\circ\text{C}$ , respectively. Fructose was detected by the RI detector; small-molecule carboxylic acids, such as FA, AA, and LA, were detected by a UV detector at a wavelength of 210 nm, and HMF was detected by a UV detector at a wavelength of 284 nm. The yields of products were determined by comparison with standard calibration curves obtained for authentic chemicals at different concentrations. The gaseous products were collected with an air trap and analyzed by means of GC-TCD (9710, Fuji) with a carbon molecular sieve packed column (TDX-1, Agilent). The oven temperature was  $120^\circ\text{C}$  and the detector temperature was  $160^\circ\text{C}$ .

The conversion of reactant ( $X$ ) and yield ( $Y$ ) were defined by Equations (6) and (7), respectively.

$$X [\text{mol } \%] = \frac{\text{moles of Fru reacted}}{\text{moles of starting Fru}} \times 100 \% \quad (6)$$

$$Y [\text{mol } \%] = \frac{\text{moles of products detected}}{\text{moles of starting Fru}} \times 100 \% \quad (7)$$

Because the carbon balance of the feedstock was low, we defined two parameters to demonstrate the origin of low carbon balance. According to quantitative analysis by HPLC, the actual carbon balance (ACB) was defined as the molar ratio between carbon detected in products and carbon added as a reactant [Eq. (8)].

$$\text{ACB} [\text{mol } \%] = \frac{\text{output of carbon}}{\text{input of carbon}} \times 100 \% \quad (8)$$

For the degradation of fructose, the generation of one mole of FA, AA, or LA resulted in the formation of one mole of degraded fructose containing five, four, or one moles of carbon atoms in the structure. This degraded fructose was hard to detect by HPLC but would undergo further condensation with other fructose or partly dehydrated fructose molecules to produce oligomers, thereby resulting in the loss of carbon in the feedstock. Assuming that the lost carbon merely came from the degradation of fructose, a theoretical carbon balance (TCB) could be calculated from Equation (9).

$$\text{TCB} [\text{mol } \%] = \frac{\text{carbon output} + \text{carbon in degraded Fru}}{\text{input of carbon}} \times 100 \% \quad (9)$$

Based on these two definitions, the difference between the theoretical carbon balance and the actual carbon balance was an indicator of whether humins were generated through the degradation polymerization route or not. If the theoretical carbon balance was equal to the actual carbon balance, then no degradation polymerization occurred. Instead, a higher theoretical carbon balance than that of the actual carbon balance was indicative of the formation of humins through degradative condensation of fructose.

## ESI-MS/MS spectra

ESI-MS/MS (LCMS-IT-TOF, Shimadzu) spectra were used to analyze the possible chemical structures of liquid products after reacting fructose at 120 °C in various solvents. The operating parameters were as follows: ionization voltage, 4.5 kV; interface temperature, 250 °C; nebulizer gas flow, 90 L h<sup>-1</sup> (N<sub>2</sub>); detector voltage, 1.60 kV; continuum mode.

## In situ ATR-IR spectra

In situ ATR-IR spectra were used to monitor the dissolution and tautomeric transformation of fructose during heating at 120 °C in various solvents. The ATR-IR spectra were collected by the ReactIR iC10 system (Mettler Toledo) equipped with a liquid-nitrogen-cooled mercury cadmium telluride (MCT) detector used for acquisition.<sup>[31]</sup> The IR signals were acquired in the range of 650–4000 cm<sup>-1</sup> through the Happ–Genzel apodization method at a resolution of 4 cm<sup>-1</sup>. Reaction profiles were generated from those data by taking band heights and given as absorbance units relative to zero. In the in situ ATR-IR experiments, the solvent was first heated to a constant temperature of 120 °C before fructose was added. After acquiring the background IR band of the given solvent at 120 °C, solid fructose was quickly transferred into the hot solvent followed by acquiring the in situ ATR-IR spectra over time.

## Quantum chemical calculations

Theoretical calculations of the IR spectra were performed by using Gaussian 09 software at the B3LYP/6-31+G(d,p) level of theory with the implicit solvation PCM and scaled by 0.9648.<sup>[16b,32]</sup> The interaction between fructose and solvent molecules in various solvents were calculated at the pbepbe/maug-cc-pvdz level of theory with the implicit solvation PCM using Gaussian 09 software.<sup>[33a–e]</sup> The PBE function was proven to predict the strength of hydrogen bonds with an accuracy of 1 kcal mol<sup>-1</sup>.<sup>[34]</sup> The D3 version of Grimme's dispersion with Becke–Johnson damping<sup>[35a,b]</sup> invoked by the "GD3BJ" keyword was employed. The density fitting approximation was employed to take advantage of the linear scaling algorithms.<sup>[36]</sup> Density fitting sets were automatically from the atomic orbital primitives within the basis set.

## Acknowledgements

We acknowledge financial support from the National Natural Science Foundation of China (no. 21875149), the 111 project (B17030), and the Basal Research Fund of the Central University (2016SCU04B06).

## Conflict of interest

The authors declare no conflict of interest.

**Keywords:** degradative condensation • fructose • humins • solvent effects • tautomerism

[1] D. Esposito, M. Antonietti, *Chem. Soc. Rev.* **2015**, *44*, 5821–5835.

[2] a) L. T. Mika, E. Csefalvai, A. Nemeth, *Chem. Rev.* **2018**, *118*, 505–613;

b) M. J. Climent, A. Corma, S. Iborra, *Green Chem.* **2011**, *13*, 520–540.

- [3] a) R.-J. van Putten, J. C. van der Waal, E. de Jong, C. B. Rasrendra, H. J. Heeres, J. G. de Vries, *Chem. Rev.* **2013**, *113*, 1499–1597; b) T. Wang, M. W. Nolte, B. H. Shanks, *Green Chem.* **2014**, *16*, 548–572; c) S. P. Teong, G. Yi, Y. Zhang, *Green Chem.* **2014**, *16*, 2015–2026.
- [4] a) G. Yong, Y. Zhang, J. Y. Ying, *Angew. Chem. Int. Ed.* **2008**, *47*, 9345–9348; *Angew. Chem.* **2008**, *120*, 9485–9488; b) I. K. M. Yu, D. C. W. Tsang, *Bioresour. Technol.* **2017**, *238*, 716–732.
- [5] A. H. Motagamwala, K. Huang, C. T. Maravelias, J. A. Dumesic, *Energy Environ. Sci.* **2019**, *12*, 2212–2222.
- [6] a) I. V. Sumerskii, S. M. Krutov, M. Y. Zarubin, *Russ. J. Appl. Chem.* **2010**, *83*, 320–327; b) S. J. Dee, A. T. Bell, *ChemSusChem* **2011**, *4*, 1166–1173; c) S. Reiche, N. Kowalew, R. Schlögl, *ChemPhysChem* **2015**, *16*, 579–587.
- [7] a) G. Tsilomelekis, M. J. Orella, Z. Lin, Z. Cheng, W. Zheng, V. Nikolakis, D. G. Vlachos, *Green Chem.* **2016**, *18*, 1983–1993; b) M. Sevilla, A. B. Fuertes, *Chem. Eur. J.* **2009**, *15*, 4195–4203; c) V. Maruani, S. Narayanan-Richenapin, E. Framery, B. Andrioletti, *ACS Sustainable Chem. Eng.* **2018**, *6*, 13487–13493; d) Z. Cheng, J. L. Everhart, G. Tsilomelekis, V. Nikolakis, B. Saha, D. G. Vlachos, *Green Chem.* **2018**, *20*, 997–1006.
- [8] K. I. Galkin, E. A. Krivodaeva, L. V. Romashov, S. S. Zaleskii, V. V. Kachala, J. V. Burykina, V. P. Ananikov, *Angew. Chem. Int. Ed.* **2016**, *55*, 8338–8342; *Angew. Chem.* **2016**, *128*, 8478–8482.
- [9] a) S. K. R. Patil, J. Heltzel, C. R. F. Lund, *Energy Fuels* **2012**, *26*, 5281–5293; b) S. K. R. Patil, C. R. F. Lund, *Energy Fuels* **2011**, *25*, 4745–4755; c) I. van Zandvoort, Y. Wang, C. B. Rasrendra, E. R. H. van Eck, P. C. A. Bruijninx, H. J. Heeres, B. M. Weckhuysen, *ChemSusChem* **2013**, *6*, 1745–1758; d) I. van Zandvoort, E. J. Koers, M. Weingarth, P. C. A. Bruijninx, M. Baldus, B. M. Weckhuysen, *Green Chem.* **2015**, *17*, 4383–4392; e) S. Karwa, V. M. Gajiwala, J. Heltzel, S. K. R. Patil, C. R. F. Lund, *Catal. Today* **2016**, *263*, 16–21.
- [10] a) L. Wang, H. Wang, F. Liu, A. Zheng, J. Zhang, Q. Sun, J. P. Lewis, L. Zhu, X. Meng, F. Xiao, *ChemSusChem* **2014**, *7*, 402–406; b) Z. Yang, W. Qi, R. Huang, J. Fang, R. Su, Z. He, *Chem. Eng. J.* **2016**, *296*, 209–216; c) L. Zhu, J. Dai, M. Liu, D. Tang, S. Liu, C. Hu, *ChemSusChem* **2016**, *9*, 2174–2181; d) J. Dai, L. Zhu, D. Tang, X. Fu, J. Tang, X. Guo, C. Hu, *Green Chem.* **2017**, *19*, 1932–1939; e) X. Guo, J. Tang, B. Xiang, L. Zhu, H. Yang, C. Hu, *ChemCatChem* **2017**, *9*, 3218–3225.
- [11] a) K.-i. Shimizu, R. Uozumi, A. Satsuma, *Catal. Commun.* **2009**, *10*, 1849–1853; b) Y. Yang, C. Hu, M. M. Abu-Omar, *Green Chem.* **2012**, *14*, 509–513; c) X. Tong, Y. Li, *ChemSusChem* **2010**, *3*, 350–355.
- [12] J. Tang, L. Zhu, X. Fu, J. Dai, X. Guo, C. Hu, *ACS Catal.* **2017**, *7*, 256–266.
- [13] a) T. D. Swift, C. Bagia, V. Choudhary, G. Peklaris, V. Nikolaldis, D. G. Vlachos, *ACS Catal.* **2014**, *4*, 259–267; b) T. D. Swift, H. Nguyen, A. Anderko, V. Nikolakis, D. G. Vlachos, *Green Chem.* **2015**, *17*, 4725–4735; c) T. D. Swift, H. Nguyen, Z. Erdman, J. S. Kruger, V. Nikolakis, D. G. Vlachos, *J. Catal.* **2016**, *333*, 149–161.
- [14] a) A. Ranoux, K. Djanashvili, I. W. C. E. Arends, U. Hanefeld, *ACS Catal.* **2013**, *3*, 760–763; b) C. Antonetti, M. Melloni, D. Licursi, S. Fulignati, E. Ribechini, S. Rivas, J. Carlos Parajo, F. Cavani, A. M. R. Galletti, *Appl. Catal. B* **2017**, *206*, 364–377; c) J. Lu, Y. Yan, Y. Zhang, Y. Tang, *RSC Adv.* **2012**, *2*, 7652–7655; d) T. Flannelly, M. Lopes, L. Kupiainen, S. Dooley, J. J. Leahy, *RSC Adv.* **2016**, *6*, 5797–5804; e) F. S. Asghari, H. Yoshida, *Ind. Eng. Chem. Res.* **2006**, *45*, 2163–2173; f) L. Qi, Y. F. Mui, S. W. Lo, M. Y. Lui, G. R. Akien, I. T. Horvath, *ACS Catal.* **2014**, *4*, 1470–1477.
- [15] a) Z. Zhang, J. Song, B. Han, *Chem. Rev.* **2017**, *117*, 6834–6880; b) Y. Roman-Leshkov, J. N. Chheda, J. A. Dumesic, *Science* **2006**, *312*, 1933–1937; c) M. A. Mellmer, C. Sanpitakseree, B. Demir, P. Bai, K. Ma, M. Neurock, J. A. Dumesic, *Nat. Catal.* **2018**, *1*, 199–207; d) T. W. Walker, A. K. Chew, H. Li, B. Demir, Z. C. Zhang, G. W. Huber, R. C. Van Lehn, J. A. Dumesic, *Energy Environ. Sci.* **2018**, *11*, 617–628; e) M. A. Mellmer, C. Sener, J. M. R. Gallo, J. S. Luterbacher, D. M. Alonso, J. A. Dumesic, *Angew. Chem. Int. Ed.* **2014**, *53*, 11872–11875; *Angew. Chem.* **2014**, *126*, 12066–12069; f) M. Benoit, Y. Brissonnet, E. Guélou, K. De Oliveira Vigier, J. Barraud, F. Jérôme, *ChemSusChem* **2010**, *3*, 1304–1309; g) Q. Zhang, K. D. O. Vigier, S. Royer, F. Jérôme, *Chem. Soc. Rev.* **2012**, *41*, 7108–7146.
- [16] a) A. S. Amarasekara, L. D. Williams, C. C. Ebede, *Carbohydr. Res.* **2008**, *343*, 3021–3024; b) G. Tsilomelekis, T. R. Josephson, V. Nikolakis, S. Caratzoulas, *ChemSusChem* **2014**, *7*, 117–126; c) X. Hu, S. Wang, R. J. M. Westerhof, L. Wu, Y. Song, D. Dong, C.-Z. Li, *Fuel* **2015**, *141*, 56–63; d) L. Ren, L. Zhu, T. Qi, J. Tang, H. Yang, C. Hu, *ACS Catal.* **2017**, *7*, 2199–2212; e) B. Xiang, Y. Wang, T. Qi, H. Yang, C. Hu, *J. Catal.* **2017**, *352*,

- 586–598; f) L. Filiciotto, A. M. Balu, J. C. Van der Waal, R. Luque, *Catal. Today* **2018**, *302*, 2–15.
- [17] a) J. J. Varghese, S. H. Mushrif, *React. Chem. Eng.* **2019**, *4*, 165–206; b) G. S. Svenningsen, R. Kumar, C. E. Wyman, P. Christopher, *ACS Catal.* **2018**, *8*, 5591–5600; c) K. Shi, C. M. Pedersen, Z. Guo, Y. Li, H. Zheng, Y. Qiao, T. Hu, Y. Wang, *J. Mol. Liq.* **2018**, *271*, 926–932.
- [18] a) T. Barclay, M. Ginic-Markovic, M. R. Johnston, P. Cooper, N. Petrovsky, *Carbohydr. Res.* **2012**, *347*, 136–141; b) H. Kimura, M. Nakahara, N. Matubayasi, *J. Phys. Chem. A* **2011**, *115*, 14013–14021.
- [19] H. Kimura, M. Nakahara, N. Matubayasi, *J. Phys. Chem. A* **2013**, *117*, 2102–2113.
- [20] a) G. R. Akien, L. Qi, I. T. Horvath, *Chem. Commun.* **2012**, *48*, 5850–5852; b) G. Yang, E. A. Pidko, E. J. M. Hensen, *J. Catal.* **2012**, *295*, 122–132; c) M. H. Tucker, R. Alamillo, A. J. Crisci, G. M. Gonzalez, S. L. Scott, J. A. Dumesic, *ACS Sustainable Chem. Eng.* **2013**, *1*, 554–560.
- [21] See the Supporting Information for details.
- [22] X. Fu, J. Dai, X. Guo, J. Tang, L. Zhu, C. Hu, *Green Chem.* **2017**, *19*, 3334–3343.
- [23] M. R. Whitaker, A. Parulkar, P. Ranadive, R. Joshi, N. A. Brunelli, *ChemSusChem* **2019**, *12*, 2211–2219.
- [24] a) Z. Tang, W. Deng, Y. Wang, E. Zhu, X. Wan, Q. Zhang, Y. Wang, *ChemSusChem* **2014**, *7*, 1557–1567; b) J. Li, D. Ding, L. Deng, Q. Guo, Y. Fu, *ChemSusChem* **2012**, *5*, 1313–1318.
- [25] Z. Jiang, J. Fan, V. L. Budarin, D. J. Macquarrie, Y. Gao, T. Li, C. Hu, J. H. Clark, *Sustainable Energy Fuels* **2018**, *2*, 936–940.
- [26] I.-E. Ortiz Cerda, P. Thammavong, V. Caqueret, C. Porte, I. Mabile, J. M. Garcia Fernandez, M. Moscosa Santillan, J.-L. Havet, *J. Agric. Food Chem.* **2018**, *66*, 1693–1700.
- [27] a) Y. Huang, P. Chao, T. Cheng, Y. Ho, C. Lin, H. Hsu, J. Wong, T. Tsai, *Chem. Eng. J.* **2016**, *283*, 778–788; b) T. Cheng, P. Chao, Y. Huang, C. Li, H. Hsu, Y. Chao, T. Tsai, *Microporous Mesoporous Mater.* **2016**, *233*, 148–153.
- [28] V. Yaylayan, A. Ismail, *J. Carbohydr. Chem.* **1992**, *11*, 149–158.
- [29] M. B. Fusaro, V. Chagnault, D. Postel, *Carbohydr. Res.* **2015**, *409*, 9–19.
- [30] H. Kishida, F. Jin, X. Yan, T. Moriya, H. Enomoto, *Carbohydr. Res.* **2006**, *341*, 2619–2623.
- [31] J. Tang, X. Guo, L. Zhu, C. Hu, *ACS Catal.* **2015**, *5*, 5097–5103.
- [32] L. Yang, G. Tsilomelekis, S. Caratzoulas, D. G. Vlachos, *ChemSusChem* **2015**, *8*, 1334–1341.
- [33] a) J. P. Perdew, K. Burke, M. Ernzerhof, *Phys. Rev. Lett.* **1996**, *77*, 3865–3868; b) J. P. Perdew, K. Burke, M. Ernzerhof, *Phys. Rev. Lett.* **1997**, *78*, 1396; c) E. Papajak, J. Zheng, X. Xu, H. R. Leverentz, D. G. Truhlar, *J. Chem. Theory Comput.* **2011**, *7*, 3027–3034; d) J. Tomasi, B. Mennucci, R. Cammi, *Chem. Rev.* **2005**, *105*, 2999–3093; e) Gaussian 09, Revision v9.5, M. J. Frisch, G. W. Trucks, H. B. Schlegel, G. E. Scuseria, M. A. Robb, J. R. Cheeseman, G. Scalmani, V. Barone, G. A. Petersson, H. Nakatsuji, X. Li, M. Caricato, A. Marenich, J. Bloino, B. G. Janesko, R. Gomperts, B. Mennucci, H. P. Hratchian, J. V. Ortiz, A. F. Izmaylov, J. L. Sonnenberg, D. Williams-Young, F. Ding, F. Lipparini, F. Egidi, J. Goings, B. Peng, A. Petrone, T. Henderson, D. Ranasinghe, V. G. Zakrzewski, J. Gao, N. Rega, G. Zheng, W. Liang, M. Hada, M. Ehara, K. Toyota, R. Fukuda, J. Hasegawa, M. Ishida, T. Nakajima, Y. Honda, O. Kitao, H. Nakai, T. Vreven, K. Throssell, J. A. Montgomery, Jr., J. E. Peralta, F. Ogliaro, M. Bearpark, J. J. Heyd, E. Brothers, K. N. Kudin, V. N. Staroverov, T. Keith, R. Kobayashi, J. Normand, K. Raghavachari, A. Rendell, J. C. Burant, S. S. Iyengar, J. Tomasi, M. Cossi, J. M. Millam, M. Klene, C. Adamo, R. Cammi, J. W. Ochterski, R. L. Martin, K. Morokuma, O. Farkas, J. B. Foresman, D. J. Fox, Gaussian, Inc., Wallingford CT, **2016**.
- [34] J. Ireta, J. Neugebauer, M. Scheffler, *J. Phys. Chem. A* **2004**, *108*, 5692–5698.
- [35] a) S. Grimme, J. Antony, S. Ehrlich, H. Krieg, *J. Chem. Phys.* **2010**, *132*, 154104; b) S. Grimme, S. Ehrlich, L. Goerigk, *J. Comput. Chem.* **2011**, *32*, 1456–1465.
- [36] B. Dunlap, *J. Mol. Struct.* **2000**, *529*, 37–40.

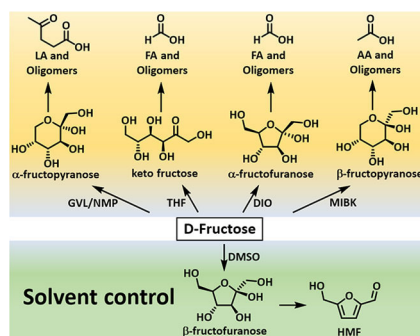
Manuscript received: August 24, 2019

Accepted manuscript online: September 26, 2019

Version of record online: ■■■■■, 0000

## FULL PAPERS

**Breaking it down:** A general understanding of the solvent-controlled formation of oligomers through the degradative condensation of fructose in the initial stage of fructose dehydration is demonstrated and reveals a close relationship between the tautomeric distribution of fructose in solvents and the degradative mechanism.



X. Fu, Y. Hu, Y. Zhang, Y. Zhang, D. Tang, L. Zhu,\* C. Hu\*



**Solvent Effects on Degradative Condensation Side Reactions of Fructose in Its Initial Conversion to 5-Hydroxymethylfurfural**

